Hindawi
International Journal of Energy Research
Volume 2023, Article ID 6696446, 12 pages
https://doi.org/10.1155/2023/6696446

Research Article

Density Functional Theory Simulation of Optical and Photovoltaic Properties of DRTB-T Donor-Based Organic Solar Cells

Daniel Dodzi Yao Setsoafia,[1] **Kiran Sreedhar Ram**,[1] **Hooman Mehdizadeh-Rad**,[1,2] **David Ompong**,[1,2] **and Jai Singh**[1,2]

[1]*Faculty of Science and Technology, Charles Darwin University, Purple 12, Darwin, NT 0909, Australia*
[2]*Energy and Resources Institute, Charles Darwin University, Darwin, NT 0909, Australia*

Correspondence should be addressed to Jai Singh; jai.singh@cdu.edu.au

Received 13 June 2023; Revised 17 August 2023; Accepted 3 September 2023; Published 19 October 2023

Academic Editor: Akshay Kumar Saha

Using the density functional theory (DFT), the influence of substitution of electron-donating (OCH_3 and OH) and electron-accepting (F and Cl) groups on the peripheral thiophene units of DRTB-T donor molecule is studied. By optimizing the geometric structure, HOMO and LUMO energies, reorganization energies, optical properties, and photovoltaic properties are simulated. It is found that the ionization potential of the electron-donating derivatives (DRTB-4OCH_3 and DRTB-4OH) reduces, but it increases for the electron-accepting derivatives (DRTB-4F and DRTB-4Cl) in comparison with that of DRTB-T. It is also found that the absorption spectra of the electron-donating derivatives (DRTB-4OCH_3 and DRTB-4OH) get redshifted, but these get blue shifted for the electron-accepting derivatives (DRTB-4F and DRTB-4Cl) in comparison with those of DRTB-T. These changes in the electronic and optical properties of the modified structures result in higher PCE in BHJ OSCs with the blended active layer of DRTB-4F: NITI, DRTB-4Cl: NITI, in comparison with that of OSC with the active layer of DRTB-T: NITI and the highest being 15.0% in DRTB-4Cl: NITI. Our results may be expected to provide valuable insights into design optimization, leading to the fabrication of more efficient OSCs.

1. Introduction

Organic solar cells (OSCs) are regarded as carbon neutral power generating devices which convert solar energy into electricity [1]. This is because OSCs possess the advantages of ease and low-cost fabrication with the potential of being used for a broad range of applications due to their flexible structure [2]. Notwithstanding these advantages, lower power conversion efficiency (PCE) and stability are major bottlenecks hindering their commercialisation [3]. Thus, research focused on designing novel active layer materials, and donor-acceptor blend configurations are aimed at higher PCE and improved stability [4].

To enhance PCE through fabrication, the bulk heterojunction (BHJ) structure first introduced by Yu et al. [5] replaced the bilayer OSC structure with a single donor-acceptor interface invented by Tang [6]. This modification enhanced PCE from 1% to 2.9% [5]. Further improvements in the choice of materials and fabrication of the BHJ structure, enhanced PCE of a BHJ OSC to more than 11% [7]. A donor (D) material usually has energetically higher frontier molecular orbitals, i.e., highest occupied molecular orbital (HOMO) and lowest unoccupied molecular orbital (LUMO) in comparison with those of acceptor (A) materials. The energy offsets at the interfaces provide the needed energy to dissociate excitons generated when a photon of

energy $E_{photon} \geq E_g$ is absorbed [8] within the blended active layer. Here, E_g is the band gap energy of the donor or acceptor used within the blend, defined as $E_g = E_{LUMO} - E_{HOMO}$ where E_{LUMO} and E_{HOMO} are the energies of LUMO and HOMO [9, 10], respectively. The excitons generated in OSCs have high binding energy due to the low dielectric constant of organic materials [11]. These excitons need to be dissociated into free electrons and holes before an OSC can generate any current. The dissociation of excitons occurs at the D-A interfaces if the energy offsets between the donor and acceptor HOMO and LUMO energies are higher than the exciton binding energy [12]. This condition also helps in choosing the donor and acceptor materials for the blend. The free charge carriers generated after the dissociation of excitons are subsequently drawn towards their respective electrodes by the electric field created by the energy difference between the work functions of anode and cathodes: holes towards anode and electrons towards cathode, and thus, such extracted charge carriers generate current in OSCs. Therefore, the availability of multiple D-A interfaces in a BHJ structure enhances the generation of free charge carriers leading to enhanced short circuit current (J_{sc}) and hence PCE. Accordingly, the search for new donor and acceptor materials with the desired HOMO and LUMO energy offsets becomes very critical in fabricating OSCs of higher PCE, which is the focus of this paper [13]. An experimental search for new materials can be expensive and time-consuming which can be avoided by searching them first through computational modelling [14–21].

It is established that all fullerene acceptor-based BHJ OSCs suffer from the low absorption and rigid molecular structure of fullerene materials [22]. Scharber [23] has reviewed PCE in OSCs and analysed that adverse energetics and recombination processes may occur within the charge transfer states (CTS) limiting their power conversion efficiency (PCE) to approximately 13%. Currently, the efficiency of only 10.4% has been attained from a BHJ structure with the blend of PffBT4T-2OD:TC_{71}BM [24]. These problems associated with the fullerene-based BHJ OSCs have led to the exploration of numerous research opportunities in the field of nonfullerene acceptor materials, which have made a significant progress in achieving a PCE surpassing 17% [15, 25]. Most of these alternative acceptor materials are polymer-based, characterized by their flexible molecular structures that facilitate easier chemical modifications to enhance absorption capabilities. However, the low stability and lack of reproducibility for the same batch of fabricated devices using the polymer donor and polymer acceptors are still the bottlenecks in achieving commercialisation of such BHJ OSCs [15]. In contrast, organic solids comprised of small molecules exhibit well-defined chemical structures that can be readily and effectively modified, ensuring minimal batch-to-batch variability in the production of OSCs [26].

Novel active layer materials based on small molecules are continually researched and developed. These molecules are designed based on the A-D-A or D-A-D configurations. These configurations create a pull-push effect within the molecule which increases the intramolecular charge transport [27–29]. However, D or A used here is not to be confused with the donor or acceptor molecule used in the blended active layer of an OSC; instead, these are the fragments within a molecule to create efficient intramolecular charge transport. The chemical functionalisation of the acceptor fragments in a A-D-A configuration has proven useful in modifying the HOMO-LUMO energy levels and absorption spectra of these molecules [19]. Most of these researches are targeted at the development of acceptor molecules to be blended within the active layer of a BHJ OSC. However, to the best of the authors' knowledge, such research developments on donor small molecules for blending within the active layer have received little or no attention in the literature. Therefore, the objective of this paper is to use the density functional theory (DFT) and time-dependent DFT (TD-DFT) to simulate five A-D-A type donor molecules for fabricating OSCs and compare the photovoltaic and quantum chemical properties of such five BHJ OSCs.

The contents of this paper are organized as follows. After the introduction presented in Section 1, Section 2 describes the theoretical details and computational procedures of simulating the photovoltaic and quantum chemical properties of BHJ OSCs. Section 3 presents the results, Section 4 includes discussions, and Section 5 draws conclusions.

2. Computational Procedures

We have chosen DRTB-T as the parent donor molecule, which has then been modified to produce four additional A-D-A configurations. These configurations involve the incorporation of two halogen atoms (F and Cl) as electron acceptors, as well as two electron-donating groups (OH and OCH_3). It is worth noting that DRTB-T, the parent donor molecule, was synthesized by Yang et al. [30], and it already possesses an A-D-A character. However, by substituting the peripheral thiophene rings in DRTB-T with F, Cl, OH, and OCH_3, its A-D-A characteristics are further enhanced.

We determine the optimal structure of the above five molecules as well as that of NITI as the acceptor molecule to be used in all five OSCs through a series of self-consistent field calculations. The 2D representation of the studied donor and acceptor molecules obtained using the Molsketch program is presented in Figure 1. Initially, the Avogadro software is used to obtain a rough geometric approximation of each molecule. Next, energy minimization is carried out by Avogadro software using the universal force field (UFF) method to obtain a starting geometry for use in the DFT calculations, and finally, an iteration process is applied to obtain the optimal geometry of each molecule using the quasi-Newton method as implemented in Orca Program version 5.0.2 [31]. For achieving the optimal geometry, the Perdew–Burke–Ernzerhof exchange-correlation functional (PBE0) [32] is used to approximate the electron exchange and correlation energy (EXC) of electron density on each molecule. The electronic wave functions of all atoms are represented using the split valence polarization with diffuse function (def2-SVP) basis sets in combination with the

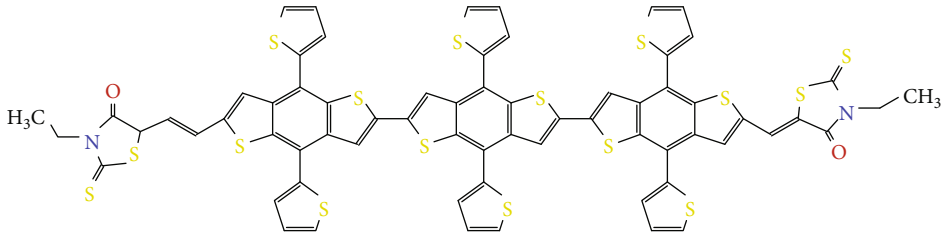

DRTB-T

(a)

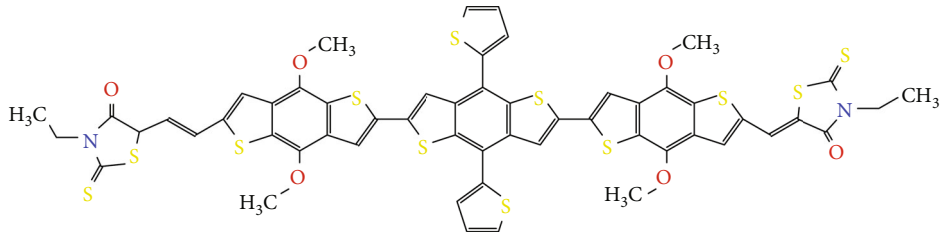

DRTB-4OCH$_3$

(b)

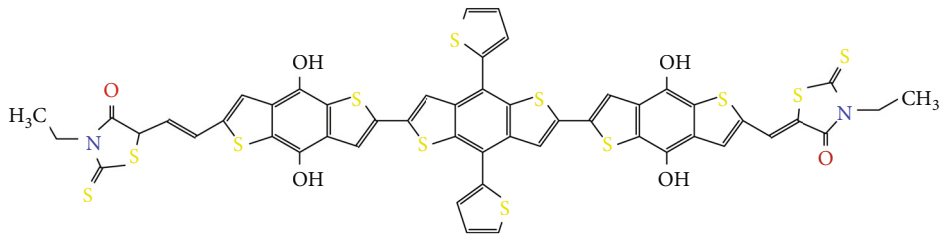

DRTB-4OH

(c)

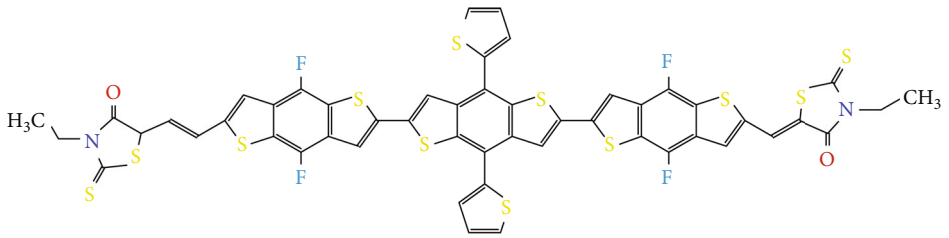

DRTB-4F

(d)

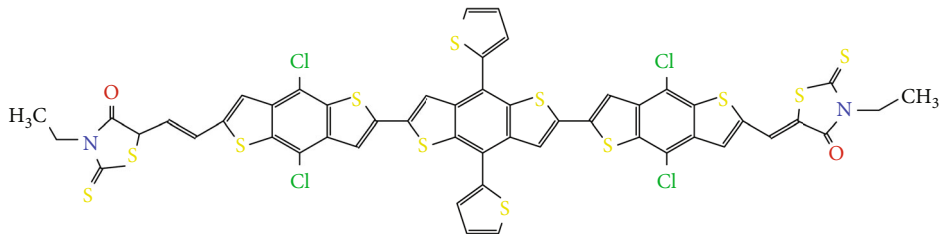

DRTB-4Cl

(e)

Figure 1: Continued.

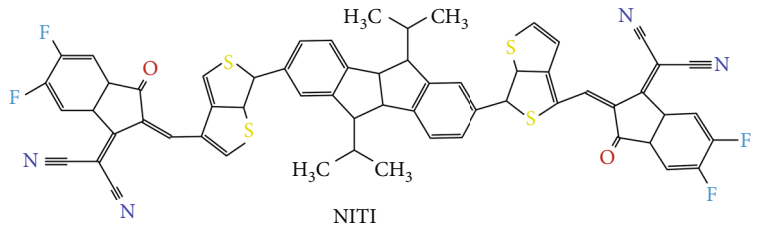

NITI

(f)

Figure 1: Structure of five donor molecules: (a) DRTB-T, (b) DRTB-4OCH3, (c) DRTB-4OH, (d) DRTB-4F, (e) DRTB-4Cl, and the acceptor molecule (f) NITI obtained using the Molsketch software.

default RI-J auxiliary basis sets. Finally, the energies of equilibrium, single point, and HOMO and LUMO are calculated for the optimized structure of each molecule and used in the evaluation of the photovoltaic and quantum chemical properties as described below.

3. Results

3.1. Geometry Optimization, HOMO and LUMO Energies, and Electronic Density Maps. The optimized structures thus obtained of the parent donor DRTB-T, its four derivatives designed by the incorporation of OCH_3, OH, F, and Cl, and the acceptor NITI molecule are shown in Figures 2(a)–2(f), respectively. Thus, the above five A-D-A type donor molecules and one acceptor molecule of NITI are used to design the active layer of five BHJ OSCs in this paper. The energies of the HOMO and LUMO of all six optimized structures obtained from the calculations are given in Table 1, along with the corresponding experimental values for comparison. The calculated HOMO and LUMO energies of DRTB-T and those of acceptor NITI are found to be in reasonable agreement with their known experimental values. The torsional angles for all donor molecules are nearly 180 degrees, indicating high planarity. Figure 3 shows the torsional angles only for the parent donor molecule DRTB-T, but other molecules are also found to have similar torsional angles.

The electronic density maps of HOMO and LUMO of the five donor molecules, DRTB-T, DRTB-4OCH_3, DRTB-4OH, DRTB-4Cl, and DRTB-4F, and those of the acceptor molecule NITI obtained by the DFT/PBE0 method with the def2-SVP basis set are shown in Figure 4.

3.2. Chemical Reactivity and Reorganization Energies. Using the calculated energies of HOMO and LUMO given in Table 1, the bandgap (E_g), ionization potential (IP), electron affinity (EA), chemical potential (CP), electronegativity (χ), softness (S), and hardness (η) are obtained as [34]

$$E_g = E_{\text{LUMO}} - E_{\text{HOMO}}, \tag{1}$$

$$\text{IP} = -E_{\text{HOMO}}, \tag{2}$$

$$\text{EA} = -E_{\text{LUMO}}, \tag{3}$$

$$\mu = \frac{E_{\text{HOMO}} + E_{\text{LUMO}}}{2}, \tag{4}$$

$$\chi = \frac{(\text{IP} + \text{EA})}{2}, \tag{5}$$

$$\eta = \frac{E_{\text{LUMO}} - E_{\text{HOMO}}}{2} = \frac{E_g}{2}, \qquad S = \frac{1}{\eta}. \tag{6}$$

The charge transport capability of a molecule is measured in terms of its reorganization energy (RE) given by [28].

$$\text{RE} = \text{RE}_e + \text{RE}_h, \tag{7}$$

where RE_e and RE_h are the reorganization energies of electrons (e) and holes (h), respectively, and these are given by

$$\text{RE}_e = (E_0^- - E_-^-) + (E_-^0 - E_0^0), \tag{8}$$

$$\text{RE}_h = (E_0^+ - E_+^+) + (E_+^0 - E_0^0), \tag{9}$$

where E_0^0 is the single point energy (SPE) of a molecule, E_0^- is SPE of the corresponding anion state. E_-^- is SPE of anionic state of an anion molecule, E_-^0 is SPE of an anion, E_0^+ is SPE of a cation, E_+^+ is SPE of the corresponding cation state, and E_+^0 is SPE a cation. All the above energies are calculated for the optimized geometries shown in Figure 2.

3.3. Optical Properties. The absorption spectra of all six molecules and corresponding oscillator strength (f) are also simulated using the TD-DFT method at the PBE0/def2-SVP level of theory. The light harvesting efficiency (LHE) of molecules is then computed as [35].

$$\text{LHE} = 1 - 10^{-f}. \tag{10}$$

The calculated absorption spectra of all the molecules plotted as a function of the spectral wavelength (λ) are shown in Figure 5, which illustrates that the absorption mainly occurs in two regions of the spectral wavelengths. The first is a weaker absorption region found in the higher energy violet-to-blue region of the solar spectrum, and the second, relatively much stronger absorption, is in the lower energy range and falls within the green-to-red region. The calculated percentage of contribution to the absorption from the transition from HOMO (H) to LUMO (L), corresponding transition energy or absorption energy, the maximum

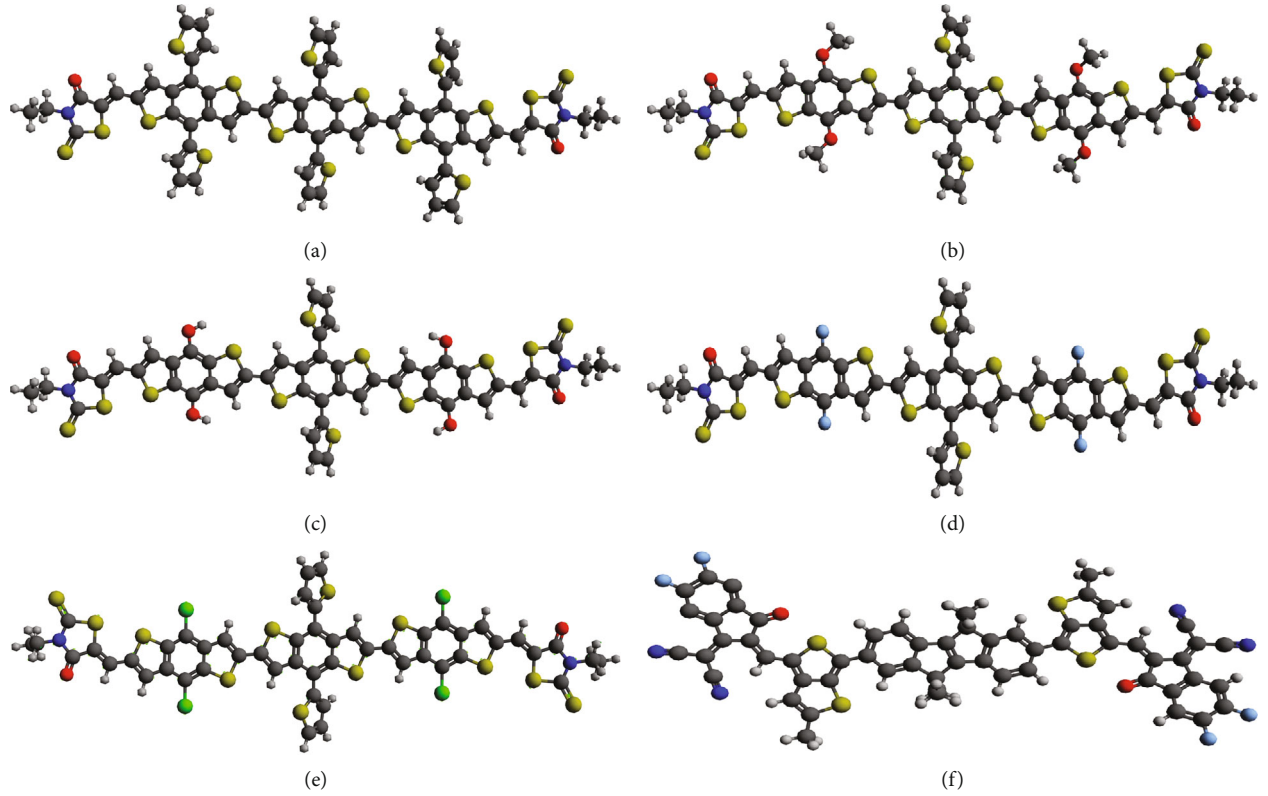

Figure 2: DFT-optimized geometries of the five donor molecules: (a) DRTB-T, (b) DRTB-4OCH$_3$, (c) DRTB-4OH, (d) DRTB-4F, (e) DRTB-4Cl, and (f) acceptor molecule of NITI.

Table 1: The energies of HOMO and LUMO of all six molecules and the corresponding energy gap E_g calculated by DFT at PBE0 level of theory for the optimized structures shown in Figure 2.

Molecules	HOMO (eV)	LUMO (eV)	HOMO (exp) (eV)	LUMO (exp) (eV)	E_g (eV)
DRTB-T	-5.64	-3.01	-5.51	-3.34 [30]	2.63
DRTB-4OCH3	-5.43	-2.97	—	—	2.46
DRTB-4OH	-5.56	-3.00	—	—	2.56
DRTB-4F	-5.85	-3.14	—	—	2.71
DRTB-4Cl	-5.86	-3.20			2.66
NITI	-6.00	-4.52	-5.68	-3.84 [33]	1.48

absorption wavelength (λ_{max}), LHE, and f of each molecule are given in Table 2 along with the experimental value of λ_{max} known for DRTB-T and NITI for comparison. Both calculated and experimental values agree quite well.

3.4. Photovoltaic Properties. According to the absorption spectra of the five donors shown in Figure 4, the dominant absorption occurs within the wavelength of 530 nm and 560 nm, and the absorption in the acceptor occurs at 640 nm. Thus, five BHJ OSCs can be designed with the active layer of five blends: (1) DRTB-T: NITI, (2) DRTB-4OCH$_3$: NITI, (3) DRTB-OH: NITI, (4) DRTB-4F: NITI, and (5) DRTB -4Cl: NITI. Using Table 1, the energy diagrams of active layers in these five BHJ OSCs are sketched in Figure 6. The energy offsets at the D-A interfaces within the active layer of an OSC affect both V_{oc} and J_{sc} and hence PCE. As it is well known that V_{oc} is related with the energy separation between the acceptor LUMO (E^A_{LUMO}) and donor HOMO (E^D_{HOMO}) as [37]

$$V_{oc} = \frac{1}{q}\left(\left|E^A_{\mathrm{LUMO}} - E^D_{\mathrm{HOMO}}\right|\right) - 0.3. \tag{11}$$

In Equation (11), an increase in the separation increases V_{oc}. At the same time, however, for efficient dissociation of the charge transfer (CT) excitons formed at the interfaces, the energy differences in the HOMO and LUMO of the donor and acceptor at the interfaces, $\Delta E_{\mathrm{LUMO}} = |E^D_{\mathrm{LUMO}} - E^A_{\mathrm{LUMO}}|$ and $\Delta E_{\mathrm{HOMO}} = |E^D_{\mathrm{HOMO}} - E^A_{\mathrm{HOMO}}|$, are required to be greater or equal to the binding energy of CT excitons (E_B) as [10]

$$\Delta E_{\mathrm{LUMO}} \text{ or } \Delta E_{\mathrm{HOMO}} \geq E_B. \tag{12}$$

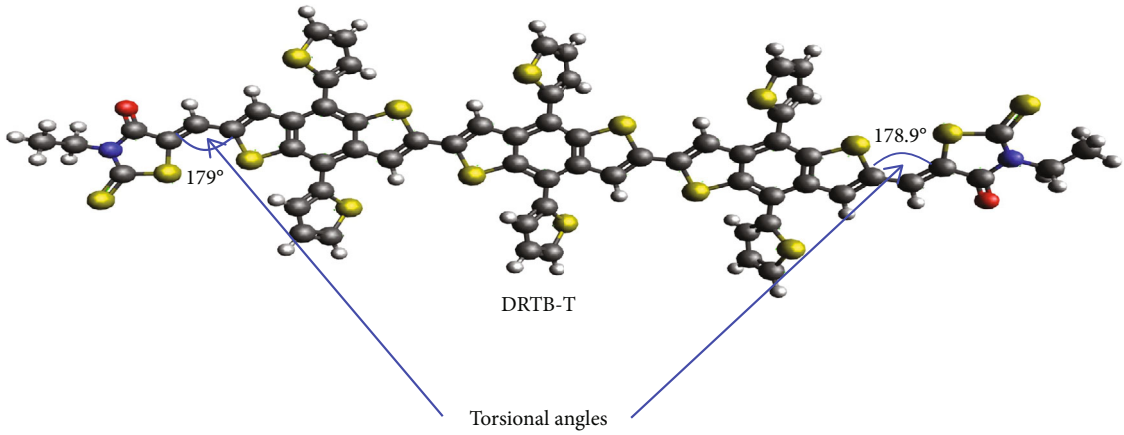

Figure 3: Calculated torsional angles between the donor and acceptor fragments in DRTB-T molecule.

Therefore, to satisfy both Equation (11) and Equation (12), one may have to compromise with obtaining both higher V_{oc} and efficient dissociation of excitons generating higher J_{sc}. This is consistent with the results obtained for the five OSCs in Table 3, which shows that the highest ΔE_{LUMO} for the OSC (2) in Figure 6 does not give the highest PCE because it produces the lowest V_{oc}. Finally, PCE of each OSC is calculated as [38]

$$\text{PCE} = \frac{J_{sc} V_{oc} \text{FF}}{P_{in}}, \tag{13}$$

where FF is the fill factor given by [39].

$$\text{FF} = \frac{qV_{oc}/K_B T - \ln\left((qV_{oc}/K_B T) + 0.72\right)}{(qV_{oc}/K_B T) + 1}. \tag{14}$$

J_{sc}, V_{oc}, FF, and PCE are thus calculated for all five OSCs and are given in Table 3. J_{sc} given in Equation (13) was calculated for each molecular blend using the procedures described by Alharbi et al. [40]. According to the absorption spectra shown in Figure 5, no significant overlap is found between any of the donor-acceptor pairs studied in this paper, and hence, no effect of overlapping is accounted for in calculating J_{sc}.

Accordingly, the OSC of DRTB-OH: NITI is found to have the lowest PCE of 9.0% and that of DRTB-4Cl: NITI has the highest PCE = 15.0%.

4. Discussions

4.1. Geometry Optimization and HOMO and LUMO Energies. The ionization potential (IP) and electron affinity (EA) of a molecule are the key parameters for determining its reactivity. Both IP and EA are directly related to HOMO and LUMO of a molecule, as IP represents the energy required to remove an electron from HOMO and EA is the amount of energy released when an electron is added to LUMO of a molecule. The calculated IP and EA of each molecule are given in Table 4, which shows that the parent donor molecule of DRTB-T has an IP = 5.64 eV and EA = 3.01 eV, and then IP of the donor molecules obtained by substitution of OH and OCH_3 decreases to 5.56 eV and 5.43 eV, respectively, and the corresponding EA also decreases to 3.00 and 2.97 eV. Thus, the incorporation of electron-donating groups of OCH_3 and OH enhances the electron-donating ability of the parent DRTB-T molecule. That means the donor molecules substituted with OH and OCH_3 can be regarded to become a better donor than the parent donor molecule of DRTB-T. Conversely, the incorporation of electron-accepting groups like F and Cl increases in DRTB-T and IP to 5.85 eV and 5.86 eV, respectively, and the corresponding EA to 3.10 eV and 3.20 eV. Accordingly, although the donors obtained from incorporating the electron-donating groups act like donors in the blended active layer of an OSC, the derivatives obtained from the electron-accepting groups act relatively as a better donor. In comparison, NITI molecule has a higher IP of 6.00 eV as well as a higher EA of 4.52 eV, which makes it a very compatible acceptor with all the five donor molecules.

The chemical potential (μ) and electronegativity (χ), calculated from Equation (4) and Equation (5), respectively, are given in Table 4 for each molecule. The chemical potential μ is a measure of the free energy available to do work by an atom or molecule [41]. In Equation (5), $\mu = -\chi$, and hence, the electronegativity becomes a measure of an atom's/molecule's ability to attract electrons towards itself when it forms a chemical bond with another atom/molecule. According to Table 4, μ values of all five donor molecules are higher than that of the acceptor NITI molecule. This means that the acceptor NITI has the lowest free energy compared to all donor molecules, and hence, electrons will easily escape from each donor to NITI when both molecules are close together. This is what is expected to occur within the active layer of any efficient BHJ OSC, i.e., efficient charge separation and collection.

The next property calculated for all the molecules is the chemical hardness η, given in Table 4, which is a measure of the molecule's ability to resist participation in a chemical reaction, including reaction with the ambient and moisture. Therefore, an organic semiconductor with a higher η can offer better stability and decreased reactivity to external agents such

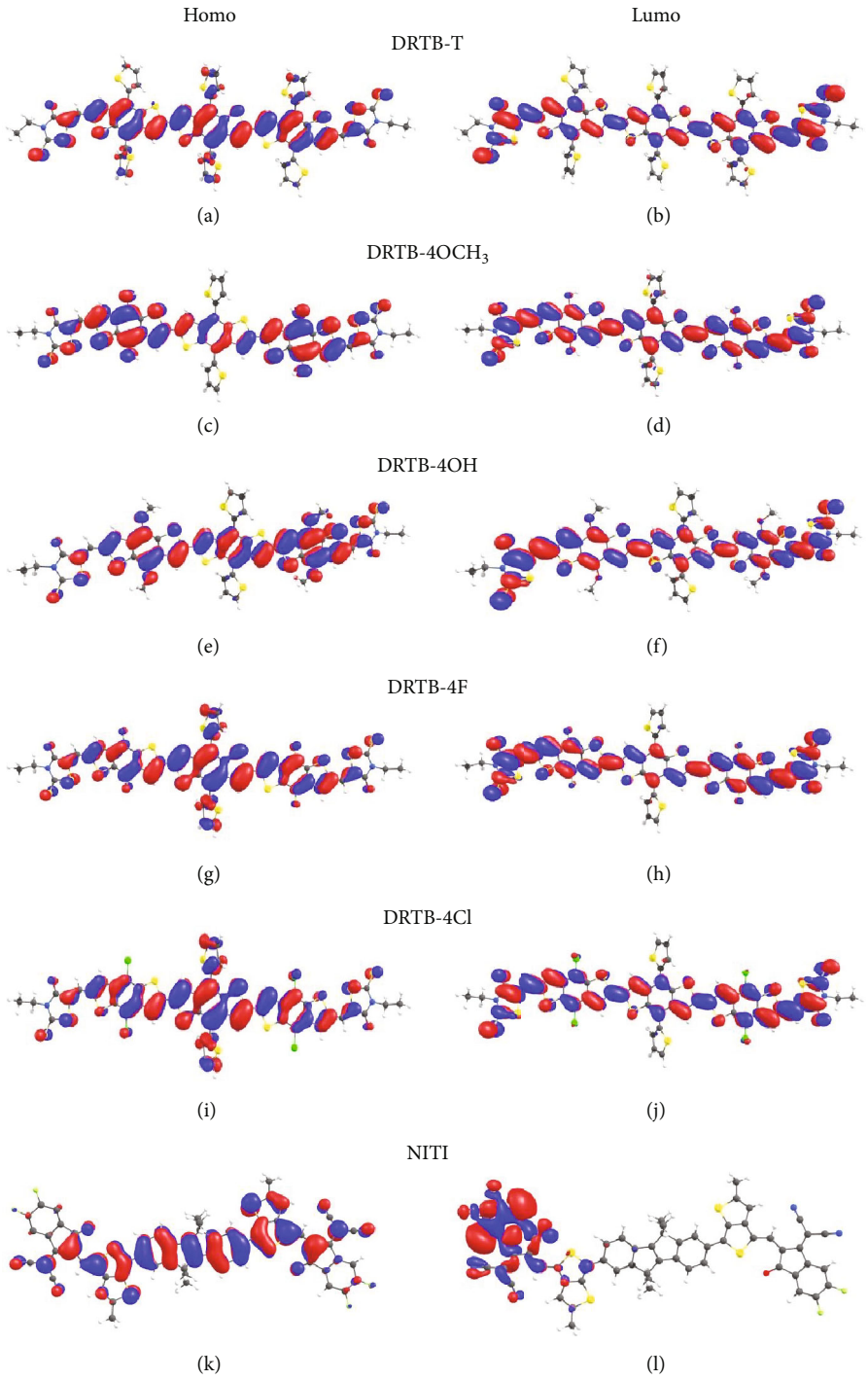

Figure 4: Electronic density maps of the HOMOs and LUMOs of donor molecules: DRTB-T (a, b), DRTB-4OCH$_3$ (c, d), DRTB-4OH (e, f), DRTB-F (g, h), DRTB-4Cl (h, j), and acceptor molecule NITI (k, l) obtained by the DFT/PBE0 method with the def2-SVP basis set.

as oxygen or water and hence should be preferably chosen for the active layer of a BHJ OSC for better stability. According to Table 4, the calculated value of η for NITI is the lowest, indicating that it is the most susceptible molecule to chemical attack. The chemical hardness of the donors given in Table 4 implies that modifying the parent donor molecule with electron-donating groups reduces the chemical hardness and hence reduces the stability, but adding electron-withdrawing groups increases chemical hardness and hence increases stability.

4.2. Reorganization Energies. Reorganization energies (RE) of a molecule are critical in determining the mobility of charge carriers in organic semiconductors. A lower value of RE generally leads to a faster charge transfer rate (K_{CT}) and higher charge carrier mobility (μ) in organic semiconductors [42].

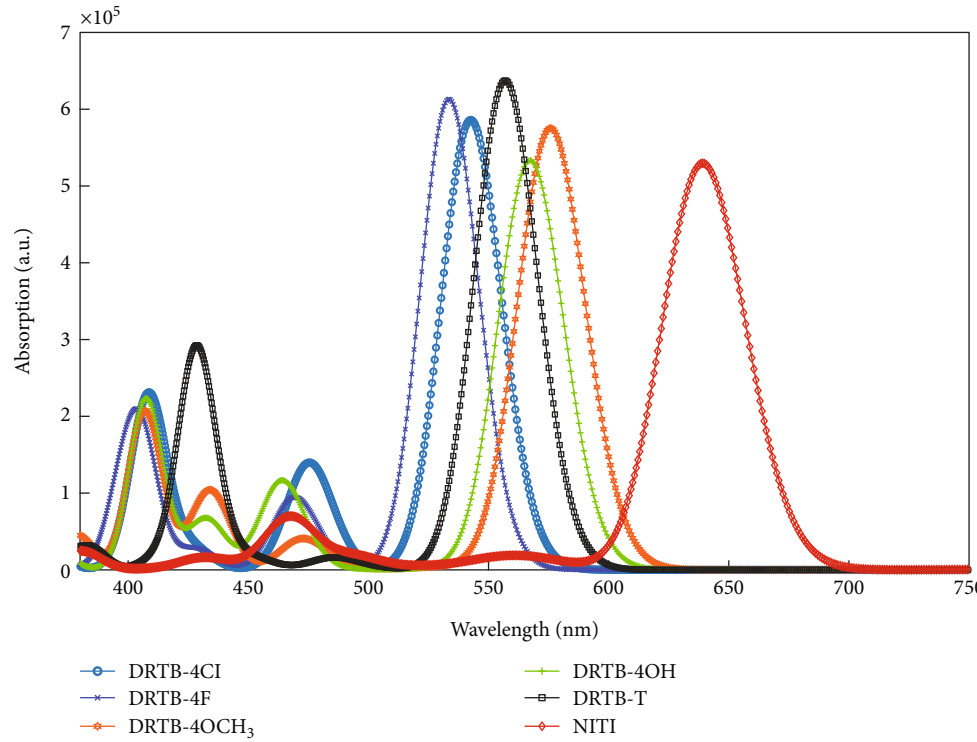

Figure 5: TD-DFT-calculated absorption of the optimized structures (shown in Figure 2) of the five donor molecules, DRTB-4Cl, DRTB-4F, DRTB-40CH3, DRTB-4OH, and DRTB-T, and the acceptor molecule of NITI.

Table 2: The calculated percentage of contribution to the absorption from the transition from HOMO (H) to LUMO (L), corresponding transition energy or absorption energy from HOMO to LUMO, and the maximum absorption wavelength (λ_{max}), LHE, and f of each molecule.

Molecules	H–L trans.	Trans. energy (eV)	Experiment λ_{max} (nm)	Calculated λ_{max} (nm)	f	LHE
DRTB-T	H⟶L 92%	2.23	545 [36]	558	2.90	0.99
DRTB-4OCH3	H⟶L 90%	2.15	—	576	2.65	0.99
DRTB-4OH	H⟶L 92%	2.19	—	567	2.45	0.99
DRTB-4F	H⟶L 97%	2.55	—	534	2.80	0.99
DRTB-4Cl	H⟶L 95%	2.30	—	543.	2.70	0.99
NITI	H⟶L 94%	1.83	719 [33]	642	2.18	0.99

However, the relationship between RE and μ is not always linear and can be influenced by other factors such as disorder or energetic barriers to charge carrier motion [43]. RE influences the degree of localization of the charge carriers. A large reorganization energy means that the charge carriers are more localized, leading to lower mobility. Conversely, a small reorganization energy promotes delocalization, which leads to higher mobility [44].

Using Equation (7), the reorganization energy (RE) is calculated and given in Table 4 for all the molecules. The incorporation of electron-donating (-OCH_3 and -OH) or electron-accepting (-F and -Cl) functional groups in DRTB-T can significantly affect RE [45] as shown in Table 4. Accordingly, the calculated RE of DRTB-4OCH_3 and DRTB-4OH is found to be lower and that of DRTB-4F and DRTB-4Cl is higher than RE of DRTB-T, the parent molecule, due to the incorporation of the electron-donating functional groups -OCH_3 and -OH. In contrast, the RE of the electron-donating molecules DRTB-4F and DRTB-4Cl are 167.4 meV and 113.4 meV, respectively, due to their reduced electron density resulting from the presence of electron-accepting groups F and Cl. Thus, a higher degree of localization is experienced by the charge carriers in DRTB-4F and DRTB-4Cl in comparison with that in DRTB-4OCH_3 and DRTB-4OH. The calculated RE of the acceptor NITI is lower than that of DRTB-T, DRTB-4F, and DRTB-4Cl, indicating the acceptor has better charge transfer but higher than the calculated RE of DRTB-OH and DRTB-OCH_3 which indicates these donors have better charge transfer. The obtained results on the effect of electron-donating and accepting groups on RE are consistent with a recent research result [46]. However, a contrary

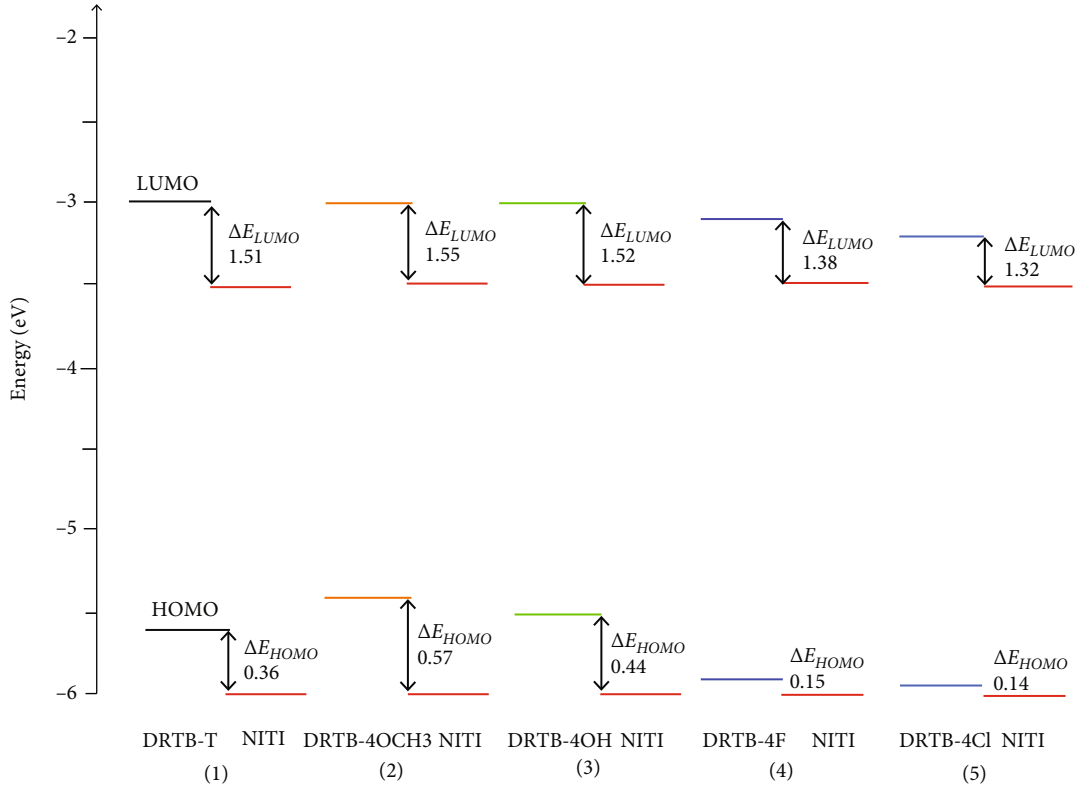

Figure 6: Energy level diagram of HOMO and LUMO and corresponding D-A energy offsets ΔE_{LUMO} and ΔE_{HOMO} for each of the five BHJ OSCs.

Table 3: Calculated J_{sc}, V_{oc}, FF, and PCE of the five BHJ OSCs studied in this paper.

Molecular blend	J_{sc} (mA/cm^2)	V_{oc} (V)	FF %	PCE %
DRTB-T: NITI	16.3	0.82	86	11.5
DRTB-4OCH3: NITI	17.7	0.61	83	9.0
DRTB-4OH: NITI	16.9	0.74	88	10.7
DRTB-4F: NITI	15.8	1.03	89	14.4
DRTB-4Cl: NITI	16.1	1.04	89	15.0

observation is also made by another research [45] suggesting that electron-withdrawing groups tend to lower the electron reorganization energy. These contrary findings suggest the complex nature of the reorganization energy and thus should motivate further research into the reorganization energy calculations for organic semiconductors prior to using in the fabrication of an OSC.

4.3. Optical Properties. The calculated absorption spectra of all six molecules in the gas phase shown in Figure 5 reveal two sets of absorption bands, one in the wavelength range of 400 to 470 nm and second in the wavelength range of 525 to 680 nm. The first absorption band in the higher energy range occurs due to intraband transitions (HOMO to HOMO or within the valence band) and hence does not contribute to the exciton generation, which requires transitions from HOMO to LUMO [47, 48]. Only the second absorption band in the lower energy range occurs due to transitions from HOMO to LUMO of each molecule and hence contributes to the photoexcitation of excitons which contribute to the charge generation and hence to the operation of an OSC fabricated from these materials.

According to Figure 5 and Table 2, the HOMO to LUMO absorption in the parent molecule of DRTB-T occurs at 558 nm. The substitution of OH and OCH_3 in DRTB-T causes a red shift in the absorption spectra to 567 nm and 576 nm, respectively, as illustrated in Figure 5. According to Table 1, this shift can be associated with the upward shift in the HOMO and LUMO energies of both the derivatives substituted with OH and OCH_3 groups. However, the red shift is slightly larger with the substitution OCH_3 than with OH (see Figure 5) and is a result of the increased electron density donated by OCH_3 than by OH which may be attributed to the resonance electron-donating effect in the methoxy group [49]. It may be noted that the effect of substitution of OCH3 on both the HOMO and LUMO energies is consistent with that observed experimentally by Li et al. [49].

However, the substitution of Cl and F in DRTB-T causes a blue shift in the absorption spectra to 543 nm and 534 nm, respectively (see Figure 5). The above-calculated spectral shifts resulting from such substitutions are apparently expected as such shifts have also been reported in other organic molecules and polymers [50, 51]. In comparison, the absorption in NITI occurs at much higher wavelength of 642 nm (see Figure 5) as required for it to be an acceptor material when blended with any of the five donor molecules.

Table 4: The calculated ionization potential (IP) for (Equation (2)), electron affinity (EA) (Equation (3), chemical potential (μ) (Equation (4)), electronegativity (χ) (Equation (5), chemical hardness (η) (Equation (6)), electron reorganization energy (RE_e) (Equation (8)), and hole reorganization energy (RE_h) (Equation (9)).

Molecules	IP (eV)	EA (eV)	η (eV)	$\mu = -\chi$ (eV)	RE_e (meV)	RE_h (meV)	RE (meV)
DRTB-T	5.64	3.01	1.32	-4.33	85.3	14.1	99.4
DRTB-4OCH$_3$	5.43	2.97	1.23	-4.20	35.0	10.1	45.1
DRTB-4OH	5.56	3.00	1.28	-4.28	25.5	13.1	38.6
DRTB-4F	5.85	3.14	1.36	-4.50	135	32.4	167.4
DRTB-4Cl	5.86	3.20	1.33	-4.530	90.3	23.1	113.4
NITI	6.00	4.52	0.74	-5.26	20.0	60.0	80.0

It is to be noted that all the main absorption bands shown in Figure 5 have high oscillator strengths in the range of 2.18-2.90 (see also Table 2). The calculated light harvesting efficiency (LHE) from Equation (10) and given in Table 2 is 0.99, close to unity for all the molecules, which implies that the absorption spectra of all the six molecules (Figure 5) result from the optimal absorption [52, 53].

4.4. Photovoltaic Properties. According to Table 3, among the simulated BHJ OSCs from the five blends of DRTB-T: NITI, DRTB-4OCH$_3$: NITI, DRTB-4OH: NITI, DRTB-4F: NITI, and DRTB-4Cl: NITI, PCE of DRTB-4Cl: NITI is the highest at 15.0%. This is because both V_{oc} and FF of DRTB-4Cl-NITI are relatively higher, and hence, in Equation (13), it gives the highest PCE. The calculated higher values of J_{sc} found in DRTB-4OCH$_3$: NITI and DRTB-4OH: NITI may be attributed to the increased gradient in electron density on the molecular blend resulting a better intramolecular charge carrier transport in these blends. Likewise, the lower J_{sc} observed in the DRTB-4F: NITI and DRTB-4Cl: NITI may be interpreted as the result of the lower gradient of electron density on these molecular blends due to the electron-accepting nature of the substituent groups.

It may be noted that FF given in Equation (14) is applicable for an ideal OSC with no series and shunt resistances. However, in a practical solar cell, these resistances are not zero, and hence, a fabricated OSC may show lower FF. This will subsequently affect the overall performance of the solar cell device. The results presented here indicate that the choice of a molecular blend for fabrication impacts the performance of OSCs significantly and hence may provide guidance in the selection of materials prior to fabrication.

5. Conclusions

This research paper presents the quantum chemical and photovoltaic properties of DRTB-T, a wide band gap donor molecule, and its four derivatives obtained by the substitution of electron-donating (-OCH$_3$ and -OH) and electron-accepting (-F and -Cl) groups at the peripheral thiophene units of DRTB-T. The findings reveal that incorporating electron-donating or electron-accepting groups influences the electron-donating ability or electron-withdrawing nature of molecules. The evaluation of geometry optimization, HOMO and LUMO energies, and reorganization energies demonstrates the importance of these substitutions in charge transfer and carrier mobility. The analysis of optical properties shows spectral shifts resulting from substitutions, affecting the absorption properties of the materials. Furthermore, the photovoltaic properties highlight the significance of the molecular blend, with the DRTB-4Cl: NITI blend achieving the highest power conversion efficiency of 15.0%. The research results of this paper may be expected to provide valuable insights into optimizing the design and performance of organic solar cells.

Data Availability

All data will be available if required.

Conflicts of Interest

The authors declare no conflict of interest.

Authors' Contributions

D.D.Y.S. carried out the details of the simulation work under the supervision of the corresponding author J.S.; H.M.R. and D.O. provided insight on using orca software, and K.S.R. helped with the literature review.

Acknowledgments

Open access publishing facilitated by Charles Darwin University, as part of the Wiley-Charles Darwin University agreement via the Council of Australian University Librarians.

References

[1] C. Xu, Z. Zhao, K. Yang et al., "Recent progress in all-small-molecule organic photovoltaics," *Journal of Materials Chemistry A*, vol. 10, pp. 6291–6329, 2022.

[2] L. Meng, M. Li, G. Lu et al., "All-small-molecule organic solar cells with efficiency approaching 16% and FF over 80," *Small*, vol. 18, no. 21, article e2201400, 2022.

[3] Y. Wang, Y. Wang, B. Kan et al., "High-performance all-small-molecule solar cells based on a new type of small molecule acceptors with chlorinated end groups," *Advanced Energy Materials*, vol. 8, no. 32, 2018.

[4] X. Wan, C. Li, M. Zhang, and Y. Chen, "Acceptor-donor-acceptor type molecules for high performance organic

photovoltaics - chemistry and mechanism," *Chemical Society Reviews*, vol. 49, pp. 2828–2842, 2020.

[5] G. Yu, J. Gao, J. C. Hummelen, F. Wudl, and A. J. Heeger, "Polymer photovoltaic cells: enhanced efficiencies via a network of internal donor-acceptor heterojunctions," *Science*, vol. 270, pp. 1789–1791, 1995.

[6] C. W. Tang, "Two-layer organic photovoltaic cell," *Applied Physics Letters*, vol. 48, pp. 183–185, 1986.

[7] H. Kang, G. Kim, J. Kim, S. Kwon, H. Kim, and K. Lee, "Bulk-heterojunction organic solar cells: five core technologies for their commercialization," *Advanced Materials*, vol. 28, pp. 7821–7861, 2016.

[8] M. Narayan and J. Singh, "A theoretical study on the operation principle of hybrid solar cells," *Electronics*, vol. 4, pp. 303–310, 2015.

[9] M. Narayan and J. Singh, "Photovoltaic contribution of photo-generated excitons in acceptor material of organic solar cells," *Journal of Materials Science: Materials in Electronics*, vol. 28, pp. 7070–7076, 2017.

[10] J. Singh, M. Narayan, D. Ompong, and F. Zhu, "Dissociation of charge transfer excitons at the donor–acceptor interface in bulk heterojunction organic solar cells," *Journal of Materials Science: Materials in Electronics*, vol. 28, pp. 7095–7099, 2017.

[11] M. R. Narayan and J. Singh, "Study of the mechanism and rate of exciton dissociation at the donor-acceptor interface in bulk-heterojunction organic solar cells," *Journal of Applied Physics*, vol. 114, article 073510, 2013.

[12] S. D. Dimitrov and J. R. Durrant, "Materials design considerations for charge generation in organic solar cells," *Chemistry of Materials*, vol. 26, no. 1, pp. 616–630, 2014.

[13] Y. Tong, Z. Xiao, X. Du et al., "Progress of the key materials for organic solar cells," *Science China Chemistry*, vol. 63, no. 6, pp. 758–765, 2020.

[14] Y. Cui, P. Zhu, X. Liao, and Y. Chen, "Recent advances of computational chemistry in organic solar cell research," *Journal of Materials Chemistry C*, vol. 8, pp. 15920–15939, 2020.

[15] G. Wang, F. S. Melkonyan, A. Facchetti, and T. J. Marks, "All-polymer solar cells: recent progress, challenges, and prospects," *Angewandte Chemie International Edition*, vol. 58, pp. 4129–4142, 2019.

[16] E. M. Speller, A. J. Clarke, N. Aristidou et al., "Toward improved environmental stability of polymer:fullerene and polymer:nonfullerene organic solar cells: a common energetic origin of light- and oxygen-induced degradation," *ACS Energy Letters*, vol. 4, no. 4, pp. 846–852, 2019.

[17] Y. Zheng, J. Huang, G. Wang et al., "A highly efficient polymer non-fullerene organic solar cell enhanced by introducing a small molecule as a crystallizing-agent," *Materials Today*, vol. 21, pp. 79–87, 2018.

[18] G. Zhang, J. Zhao, P. C. Y. Chow et al., "Nonfullerene acceptor molecules for bulk heterojunction organic solar cells," *Chemical Reviews*, vol. 118, pp. 3447–3507, 2018.

[19] D.-D.-Y. Setsoafia, K.-S. Ram, H. Mehdizadeh-Rad, D. Ompong, V. Murthy, and J. Singh, "DFT and TD-DFT calculations of orbital energies and photovoltaic properties of small molecule donor and acceptor materials used in organic solar cells," *Journal of Renewable Materials*, vol. 10, no. 10, pp. 2553–2567, 2022.

[20] M. R. S. A. Janjua, "Quantum chemical design of D–π–A-type donor materials for highly efficient, photostable, and vacuum-processed organic solar cells," *Energy Technology*, vol. 9, article 2100489, 2021.

[21] U. Yaqoob, A. Raza Ayub, S. Rafiq et al., "Structural, optical and photovoltaic properties of unfused non-fullerene acceptors for efficient solution processable organic solar cell (estimated PCE greater than 12.4%): a DFT approach," *Journal of Molecular Liquids*, vol. 341, article 117428, 2021.

[22] R. Ganesamoorthy, G. Sathiyan, and P. Sakthivel, "Review: fullerene based acceptors for efficient bulk heterojunction organic solar cell applications," *Solar Energy Materials and Solar Cells*, vol. 161, pp. 102–148, 2017.

[23] M. C. Scharber, "On the efficiency limit of conjugated polymer:fullerene-based bulk heterojunction solar cells," *Advanced Materials*, vol. 28, pp. 1994–2001, 2016.

[24] Y. Liu, J. Zhao, Z. Li et al., "Aggregation and morphology control enables multiple cases of high-efficiency polymer solar cells," *Nature Communications*, vol. 5, p. 5293, 2014.

[25] M. R. S. A. Janjua, "All-small-molecule organic solar cells with high fill factor and enhanced open-circuit voltage with 18.25% PCE: physical insights from quantum chemical calculations," *Spectrochimica Acta Part A: Molecular and Biomolecular Spectroscopy*, vol. 279, article 121487, 2022.

[26] H. Gao, Y. Sun, L. Meng, C. Han, X. Wan, and Y. Chen, "Recent progress in all-small-molecule organic solar cells," *Small*, vol. 19, article 2205594, 2023.

[27] W. Taouali, M. E. Casida, A. A. M. H. M. Darghouth, and K. Alimi, "Theoretical design of new small molecules with a low band-gap for organic solar cell applications: DFT and TD-DFT study," *Computational Materials Science*, vol. 150, pp. 54–61, 2018.

[28] M. Y. Mehboob, R. Hussain, M. Adnan et al., "Theoretical modelling of novel indandione-based donor molecules for organic solar cell applications," *Journal of Physics and Chemistry of Solids*, vol. 162, article 110508, 2022.

[29] T. Wang, R. An, M. Cao et al., "Nonfullerene acceptors with cyano-modified terminal groups for organic solar cells: effect of substitution position on photovoltaic properties," *Dyes and Pigments*, vol. 206, article 110661, 2022.

[30] L. Yang, S. Zhang, C. He et al., "New wide band gap donor for efficient fullerene-free all-small-molecule organic solar cells," *Journal of the American Chemical Society*, vol. 139, pp. 1958–1966, 2017.

[31] F. Neese, F. Wennmohs, U. Becker, and C. Riplinger, "The ORCA quantum chemistry program package," *The Journal of Chemical Physics*, vol. 152, article 224108, 2020.

[32] J. P. Perdew, M. Ernzerhof, and K. Burke, "Rationale for mixing exact exchange with density functional approximations," *The Journal of Chemical Physics*, vol. 105, pp. 9982–9985, 1996.

[33] S. J. Xu, Z. Zhou, W. Liu et al., "A twisted thieno[3,4-b]thiophene-based electron acceptor featuring a 14-π-electron indenoindene core for high-performance organic photovoltaics," *Advanced Materials*, vol. 29, article 1704510, 2017.

[34] A. Rasool, S. Zahid, M. Ans, S. Muhammad, K. Ayub, and J. Iqbal, "Bithieno thiophene-based small molecules for application as donor materials for organic solar cells and hole transport materials for perovskite solar cells," *ACS Omega*, vol. 7, pp. 844–862, 2022.

[35] W. Sang-aroon and S. Tontapha, Eds.V. Amornkitbamrung, "Chapter 6 - photovoltaic performance of natural dyes for dye-sensitized solar cells: a combined experimental and

theoretical study," in *Dye-Sensitized Solar Cells*, W. Sang-aroon, S. Tontapha, , and , Eds., pp. 203–229, Academic Press, 2019.

[36] Y. Wang, Y. Wang, L. Zhu et al., "A novel wide-bandgap small molecule donor for high efficiency all-small-molecule organic solar cells with small non-radiative energy losses," *Energy & Environmental Science*, vol. 13, pp. 1309–1317, 2020.

[37] N. K. Elumalai and A. Uddin, "Open circuit voltage of organic solar cells: an in-depth review," *Energy & Environmental Science*, vol. 9, pp. 391–410, 2016.

[38] K. S. Ram, D. Ompong, H. M. Rad, D. D. Y. Setsoafia, and J. Singh, "An alternative approach to simulate the power conversion efficiency of bulk heterojunction organic solar cells," *Physica Status Solidi (A)*, vol. 218, 2020.

[39] B. Qi and J. Wang, "Fill factor in organic solar cells," *Physical Chemistry Chemical Physics*, vol. 15, pp. 8972–8982, 2013.

[40] F. H. Alharbi, S. N. Rashkeev, F. El-Mellouhi, H. P. Lüthi, N. Tabet, and S. Kais, "An efficient descriptor model for designing materials for solar cells," *Npj Computational Materials*, vol. 1, article 15003, 2015.

[41] L.-Q. Chen, "Chemical potential and Gibbs free energy," *MRS Bulletin*, vol. 44, pp. 520–523, 2019.

[42] R. Saxena, V. R. Nikitenko, I. I. Fishchuk et al., "Role of the reorganization energy for charge transport in disordered organic semiconductors," *Physical Review B*, vol. 103, article 165202, 2021.

[43] V. Coropceanu, J. Cornil, D. A. da Silva Filho, Y. Olivier, R. Silbey, and J.-L. Brédas, "Charge transport in organic semiconductors," *Chemical Reviews*, vol. 107, pp. 926–952, 2007.

[44] S. Giannini, A. Carof, M. Ellis et al., "Quantum localization and delocalization of charge carriers in organic semiconducting crystals," *Nature Communications*, vol. 10, p. 3843, 2019.

[45] M. H. Tahir, T. Mubashir, T.-U.-H. Shah, and A. Mahmood, "Impact of electron-withdrawing and electron-donating substituents on the electrochemical and charge transport properties of indacenodithiophene-based small molecule acceptors for organic solar cells," *Journal of Physical Organic Chemistry*, vol. 32, article e3909, 2019.

[46] C.-P. Hsu, "Reorganization energies and spectral densities for electron transfer problems in charge transport materials," *Physical Chemistry Chemical Physics*, vol. 22, pp. 21630–21641, 2020.

[47] W. Bennecke, A. Windischbacher, D. Schmitt et al., "Multiorbital exciton formation in an organic semiconductor," 2003, https://arxiv.org/abs/2303.13904.

[48] M. Maimaris, A. J. Pettipher, M. Azzouzi et al., "Sub-10-fs observation of bound exciton formation in organic optoelectronic devices," *Nature Communications*, vol. 13, no. 1, p. 4949, 2022.

[49] S. Li, L. Ye, W. Zhao, S. Zhang, H. Ade, and J. Hou, "Significant influence of the methoxyl substitution position on optoelectronic properties and molecular packing of small-molecule electron acceptors for photovoltaic cells," *Advanced Energy Materials*, vol. 7, article 1700183, 2017.

[50] R. Lenaerts, D. Devisscher, G. Pirotte et al., "The effect of halogenation on PBDTT-TQxT based non-fullerene polymer solar cells - chlorination vs fluorination," *Dyes and Pigments*, vol. 181, article 108577, 2020.

[51] Y. Wang, C. Zhang, B. Yang et al., "The halogenation effects of electron acceptor ITIC for organic photovoltaic nano-heterojunctions," *Nanomaterials*, vol. 11, p. 3417, 2021.

[52] J. Preat, A. Hagfeldt, and E. A. Perpète, "Investigation of the photoinduced electron injection processes for p-type triphenylamine-sensitized solar cells," *Energy & Environmental Science*, vol. 4, pp. 4537–4549, 2011.

[53] M. Raftani, T. Abram, N. Bennani, and M. Bouachrine, "Theoretical study of new conjugated compounds with a low band-gap for bulk heterojunction solar cells: DFT and TD-DFT study," *Results in Chemistry*, vol. 2, article 100040, 2020.